Charge Transfer in Molecular Cocrystals: A Plane Wave vs Localized-Orbital View–Structural Information Obtained from Calculated Raman and IR Phonons

Charge transfer in molecular co-crystals: a plane wave vs. localized-orbitals view. Structural information obtained from calculated Raman and IR phonons.

Fabio Biffoli,[1,2]♯, Davide Vanossi,[3]♯, Elisabetta Venuti,[4] Tommaso Salzillo, [4] Marco Bonechi,[1] Massimo Innocenti,[1,5,6] Marco Pagliai,[1] and Claudio Fontanesi*[5,7]

[1]*Department of Chemistry, "Ugo Schiff", University of Firenze, via della Lastruccia 3, 50019 Sesto Fiorentino, ITALY.*

[2]*Materia Firenze Lab s.r.l., Gruppo Materia Firenze, Via delle Fonti 8/E, 50018 Scandicci (FI), Italy.*

[3]*Department of Chemical and Geological Science, DSCG, University of Modena and Reggio Emilia, via Campi 103, 41125 Modena, Italy.*

[4] *Department of Industrial Chemistry "Toso Montanari" & INSTM-UdR Bologna, Via Gobetti85, 40129 Bologna, Italy*

[5]*National Interuniversity Consortium of Materials Science and Technology (INSTM), Via G. Giusti 9, 50121 Firenze (FI), Italy.*

[6]*Center for Colloid and Surface Science (CSGI), Via della Lastruccia 3, 50019 Sesto Fiorentino (FI), Italy*

[7]*Department of Engineering "Enzo Ferrari", (DIEF), University of Modena and Reggio Emilia, Via vivarelli 10, 41125 Modena, Italy.*

Abstract

This article aims at laying the foundation for the development of electronic structure–property relationship in the field of charge-transfer (CT) organic semiconductors by studying the low-frequency phonon response of donor-acceptor (DA) compounds. In this paper, it is shown and discussed how and why phonon frequencies and their delocalization depend on the interplay between single-molecule properties and crystal structure. This result is obtained combining results from state-of-the art quantum–mechanical calculations, carried out within both localized orbitals and plane wave paradigm, with simple classical models. CT compounds between perylene (Pery) as the donor and FnTCNQ (n = 0, 4) as the acceptors, have been considered.

♯Authors D.V. and F.B. contributed equally.

Keywords: co-crystal, perylene, TCNQ, phonon, DFT

Corresponding author: claudio.fontanesi@unimore.it

Introduction

Following the seminal work of Heeger, MacDiarmid, and Shirakawa on molecularly doped conjugated polymers the scientific research based on the development of hydrocarbon-based semiconducting materials drove the development of the so-called "organic electronics" field of research activity[1–5]. In particular, semiconducting polymers are at present mainly employed in cheap and easily assembled thin film transistors[6], light emitting materials[7], and dye-sensitized solar cells (DSSC)[8]. From a purely applicative point of view, maybe the most effective manifestation of organic electronics in the impact on every-day is the production of screen and touch-screen devices for the display of monitors and smartphones. Within this picture, conjugated sulfur-containing aromatic systems, i.e. polythiophenes, remain the most popular choices for the preparation of organic electronic materials, in that they are i) typically good donors ii) the preferentially planar geometrical arrangement and the presence of 3p orbitals on sulfur atoms allows an efficient inter molecular orbital overlap. These characteristics make them very good candidates as donors in binary charge–transfer (CT) complexes[9]. Although CT complexes have long been known, their potential as electronic materials have not been noted until relatively recently, despite their capability of fine-tuning electric properties depending on heteroatoms and substituents[10]. Previous reports indicate that binary CT complexes show high conductivity and other promising optoelectronic properties such as ambipolar transport and photoconductivity[11]. The electronic properties of CT complexes have also been exploited to develop a wide variety of colorimetric sensors, based on the rising of characteristic absorption bands[12]. A comprehensive review of experimental and theoretical this topic was proposed by Pramanik *et al.*[13] In the field of CT complexes molecular crystals represent an important class of materials due the tunability of their properties strictly dependent on the crystalline structure[10,14,15].

Molecular crystals are ordered packings of molecules which are the discrete physical entities characterizing the solid. It can be seen that the forces determining the packing in molecular crystals are much weaker than those of ionic or covalent chemical bonds[16,17]. The physical nature of such weaker intermolecular forces can be used to characterize the crystal itself and its properties[18]. Among the various kinds of molecular solids, organic charge transfer crystals have attracted significant research attention due to their wide range of potential applications in organic optoelectronic devices[19], organic magnetic devices, organic energy devices, etc. In this type of solids donor-acceptor interaction occurs between "planar" donor (D) and acceptor (A) molecules packed in an infinite arrangement; to this end a crucial role is related to the energy difference of HOMO (D) and LUMO (A) orbitals.

The Born-Oppenheimer electronic ground state of such systems is partially ionic in nature and the degree of CT is largely responsible for the resulting properties of the crystal[20]. It is worthwhile to emphasize that, in systems with long range crystalline order, not only the energy difference between

HOMO and LUMO is important in determining the value of CT but also the electronic coupling between these frontier orbitals plays a crucial role[21,22]. The degree of CT can be, for example, estimated by single-crystal XRD[23] by calculating the variation in the bond length. In this study, however, we used vibrational spectroscopy (IR and Raman) to estimate the value of CT for organic charge transfer crystals : it is in fact widely recognized that charge transfer interactions influence some vibrational modes of both donor and acceptor molecules[24,25]. In parallel, theoretical studies were conducted to validate and predict experimental CTs from vibrational spectra: despite the importance of the estimation of CT, these measurements, both from an experimental and a computational point of view, lead to conflicting results[14,20,26,27]. This article aims to delve into the theoretical aspects of determining the CT, by validating and suggesting a novel and robust workflow to obtain reliable CT values for molecular crystals by an *in-silico* approach. The degree of CT and the influence of the level of theory on its estimation was benchmarked within the density functional theory (DFT), testing both localized orbitals (LO) and plane-waves (PW) and investigating the interaction between these and different population analyses. Perylene (Pery) Fn-7,7,8,8-tetracyanoquinodimethane (FnTCNQ) cocrystals were selected as prototypical organic charge transfer crystals as they have been extensively studied and characterised and still represent a system of interest because of their variety and fine-tuning possibilities[28–34]. The CT in molecular crystals is strictly linked with the electronic band structure, making the study of this variable of interest for electrochemical experiments, as the bandgap can be accessed via cyclic voltammetry, and a robust protocol to theoretically verify experimental result is necessary[27,35,36].

Experimental

CT crystals were prepared following the previously reported procedure by Salzillo et al.[20] by physical vapor transport method. THz-IR (or Far-IR) measurements have been performed with in-house setup based on a Bomem DA8 interferometer with a maximum spectral resolution of 0.004 cm^{-1} working in a final vacuum in the range of 10^{-4} mbar and equipped with Globar source water cooled, Mylar Hyperspectral beamsplitter and DTGS detector. The signal is collected in transmission mode with the samples previously dispersed in polyethylene powder (Sigma Aldrich (UHMW PE), powder, mean particle size 150 μm) and pressed at room temperature in a pellet. The pellet is prepared by dispersing about 1 mg of sample in crystal form and mixed in 60 mg of polyethylene powder by agate mortar reaching the homogenity. Each spectrum is the results of 9999 scans with 2 cm^{-1} spectral resolution and as a background a KBr spectrum recorded with the same conditions has been used. THz-Raman (or low-frequency Raman) measurements have been performed with Horiba Jobin Yvon T64000 triple grating spectrometer working in double subtractive + single additive configuration at ambient conditions. The excitation laser line was from a Krypton ion gas laser (Coherent Innova 90C) tuned at

647.1 nm and power modulated by neutral optical density filters to obtain about 1 mW on the sample to avoid its degradation. Each spectrum has been recorded with 100x objective, integrating 240 s and averaging 6 spectra. For each crystal at least 6 independent measurements have been recorded to ensure the homogeneity of the sample. The calibration of the triple spectrometer has been performed with narrow neon emission lamp.

Calculation details

Projector augmented wave (PAW) calculations with periodic boundary conditions (PBC) were performed with VASP 5.4.4 program[37,38], selecting the h_GW family of default PAW pseudopotentials[39,40] and an energy cut-off of 910 eV. The dispersion-corrected density functional theory (DFT-D) was employed with the PBE[41] exchange and correlation functional coupled with the D3(BJ) empirical correction to account for dispersion interaction[42]. Geometries and cell parameters were optimized using the conjugate-gradient method starting from experimental X-ray results[20] (the experimental geometries are attached as F0TCNQPerylene_1-1.cif and F4TCNQPerylene_1-1.cif files in the supporting information). For this work the α-polymorph with donor-acceptor stoichiometry 1:1 is considered for both species, setting as symmetry constrain the $P2_1/c$ space group for Pery:TCNQ and P-1 for Pery:F4TCNQ. For both species the k-points were Γ-centred and automatically generated. For Pery:F4TCNQ a 6 x 6 x 4 Monkhorst sampling was used, then a 5 x 3 x 3 sampling was used Pery:TCNQ. Frequency calculations were done at Γ thanks to the Phonopy package[43] with a finite difference approach (0.01 Å displacements), employing VASP 5.4.4 as force calculator. IR intensities and Raman activities were evaluated thanks to the Phonopy-spectroscopy framework[44]. A 2 x 1 x 1 supercell was needed for the Pery:F4TCNQ crystal to ensure convergence. The electronic structure of dimers was also evaluated with LOs, on the Gaussian 16[45] environment, at DFT-D level implementing again D3(BJ) empirical dispersions. Different population analyses were benchmarked to obtain atomic charges: Mulliken, Bader and DDEC6. DDEC6 charges were evaluated with chargemole[46] both for LO and PAW calculations. Mulliken charges for LOs were obtained from Gaussian 16, for PAWs, instead, the LOBSTER program was used, setting the pbeVaspFit2015 as auxiliary basis set[47]. Finally, Bader charges were processed with the Henkelman's group code[48,49] for PAWs and with Multiwfn[50] for LOs. The influence of different basis sets and functionals on population analyses was tested by varying both in LO calculations. We selected the CAM-B3LYP[51] as our high level hybrid functional and cc-pVTZ[52] as the reference basis set: various exchange and correlation functionals (BLYP[53], B3LYP[54], PBE, PBE0[55]) against the CAM-B3LYP(D3BJ)/cc-pVTZ standard. The effect of the basis set extension and the influence of polarization and diffuse functions were also tested by employing the following basis sets in conjunction with the CAM-B3LYP functional: 6-31G[56], 6-31G(d)[56,57], 6-31+G[56,58], 6-31+G(d)[56–58], 6-311G(2d,2p)[57,59], 6-311++G(2d,2p)[57–59], 6-

311++G(3df,3pd) [57–59], cc-pVDZ[60], aug-cc-pVDZ[52,60], cc-pVTZ and aug-cc-pVTZ[52]. The theoretical CT was determined by the sum of net atomic charges over a Pery molecule.

Results and Discussion

In CT complexes the central question is represented by the determination of the amount of charge transferred between the donor and the acceptor. Indeed, the crux is to devise a strategy allowing for a reliable quantitative estimation, experimentally as well as theoretically[31,61–63]. The Pery:F4TCNQ with a 1:1 stoichiometry CT co-crystal constitutes an interesting benchmark for any theoretical approach, in that experimentally from the analysis of IR spectra a charge transfer value of 0.29 electrons is obtained: with the formation of a positively charged Pery[20]. We selected the FnTCNQ (n=0, 4) from the whole series as there is no intrinsic disorder due the asymmetry of the acceptor, as for n=1, 2, 3, making these species more suitable for systematic theoretical study. Chart 1 shows the optimized crystal structure at PBE(D3BJ)/PAW level (the optimized geometries are attached as F0TCNQPerylene_1-1_opt.cif and F4TCNQPerylene_1-1_opt.cif files in the supporting information). A comparison of experimental and optimized lattice parameters is reported in Table S1 for both species, underlining a good agreement between experimental and theoretical results.

Chart 1

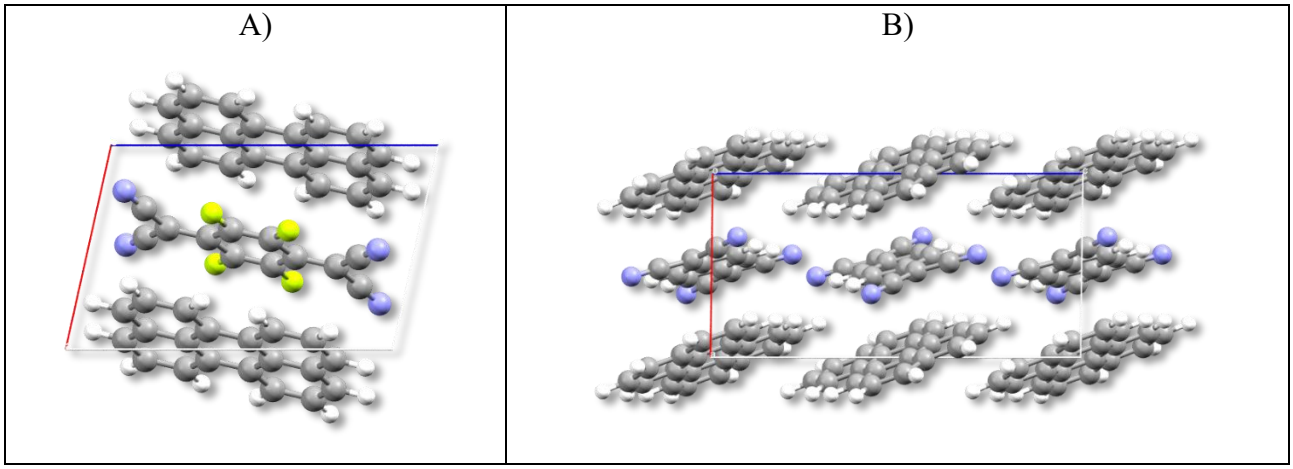

Chart 1: Optimized crystal structure at PBE(D3BJ)/PAW level of A) triclinic Pery:F4TCNQ stoichiometry 1:1 and P-1 as space group B) monoclinic Pery:TCNQ, stoichiometry 1:1 and $P2_1/c$ as space group.

Figure 1 displays the frontier orbitals correlation diagram for the isolated pristine species Pery, TCNQ, F4TCNQ, together with the relevant 1:1 stoichiometry CT complexes. In that, the driving-force of the CT process is often rationalized considering that the LUMO energy of the acceptor has to be near in energy with respect to that of the HOMO of the donor. Note that, both the donor and acceptors undergo a lowering in electronic state symmetry, passing from D_{2h} (isolated molecule) to

160 C_i (in the crystal, concerning the symmetry of the elementary cell). In order to form the donor-accep-
161 tor complex, the two species have to be arranged in a staggered manner, further lowering the sym-
162 metry of the dimer to C_1, this disposition minimizes the orthogonality between the HOMO of the
163 donor (A_g) and the LUMO of the acceptor (A_u); this geometry reduces the need for charge transfer
164 between LUMO and HOMO-1 reported in the literature for similar cases[64]. This can be observed in
165 Figure 1B where the LUMO and HOMO of F4TCNQ and Pery are combined to give a constructive
166 and destructive pattern, highlighting how the two species are positioned to avoid the orthogonality of
167 considered molecular orbitals.

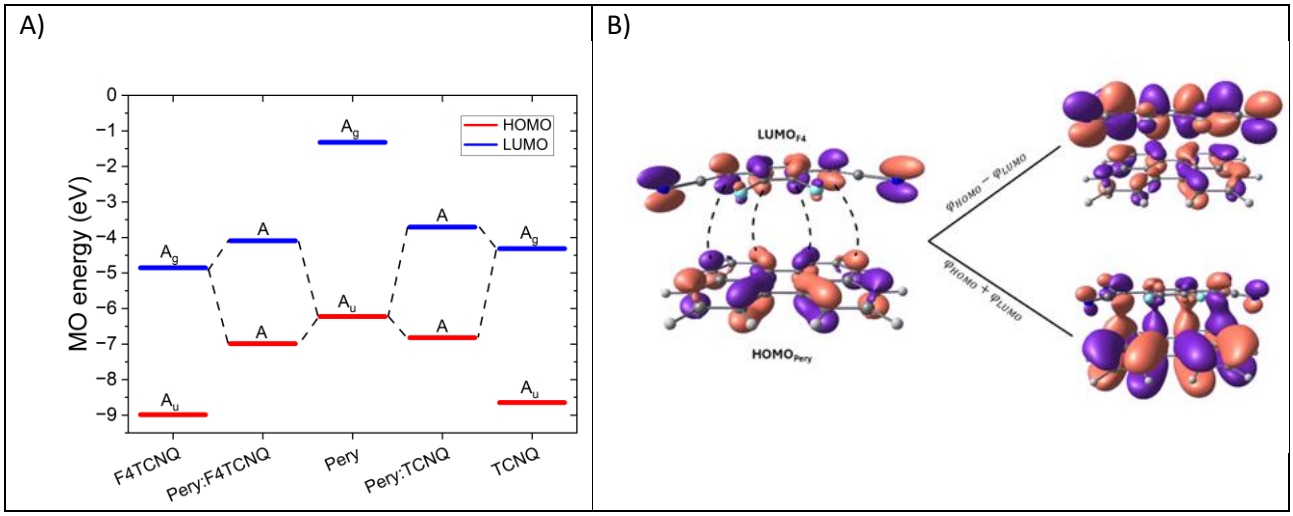

168 **Figure 1**. A) Pery, TCNQ, F4TCNQ frontier orbitals correlation diagram CAM-B3LYP(D3BJ)/cc-
169 pVTZ level of the theory. The diagram shows also the frontier orbitals of Pery:TCNQ and
170 Pery:F4TCNQ CT complexes. The calculation was performed extracting the dimer geometry from
171 the optimized structures after PAWs calculations (with PBC). B) constructive and destructive combi-
172 nation of frontiers orbital of Pery and F4TCNQ; it can be seen how the inversion centres of donor
173 and acceptor are not aligned to obviate the orthogonality between the Pery HOMO (A_u) and F4TCNQ
174 LUMO (A_g).

175

176 Figure 2 allows for a single glance comparison of theoretical and experimental IR spectra, the shift
177 in energy of the bands labelled with an asterisk, ("*", in Figure 2), is exploited for estimating exper-
178 imentally the CT. It is accomplished by comparing the corresponding vibrational bands of the neutral
179 acceptor molecule, in this case the F4 (reference vibrational energy values for the neutral F4 and F0
180 acceptor compounds are reported in Table S2). All in all, the calculated pattern shows a rather good
181 match with the data reported in the literature. This is verified also taking into account the differences
182 in the experimental IR spectra due to crystal anisotropic factors (orientation concerning the direction
183 of the incident radiation), already discussed in detail in ref[20]. The agreement between the calculated
184 (plane wave) and experimental IR spectra, strongly suggests the agreement between the optimized
185 structure and the effective crystal geometry, allowing to proceed further in the calculation of the
186 charge transfer, with 0.29 electrons as a reference value. It has to be noted that, vibrational frequencies

reported in Figure 2 are scaled by a factor of 1.02 (which will be discussed lately in the manuscript), which was determined following an error minimization procedure: calculation of the root-mean square-deviation (RMSD) between theoretical data and experimental values in the near-IR region concerning experimental data of IR spectra available for both the Pery:F0 (1:1 stoichiometry) and Pery:F4 (1:1).[14,20] This was accomplished by performing a linear regression between the marked ("*") bands and modes 130 and 133 for the Pery:F4 (1:1) and mode 256 for Pery:F0 (1:1). Unscaled frequencies are reported in Table S3, Supporting Information.

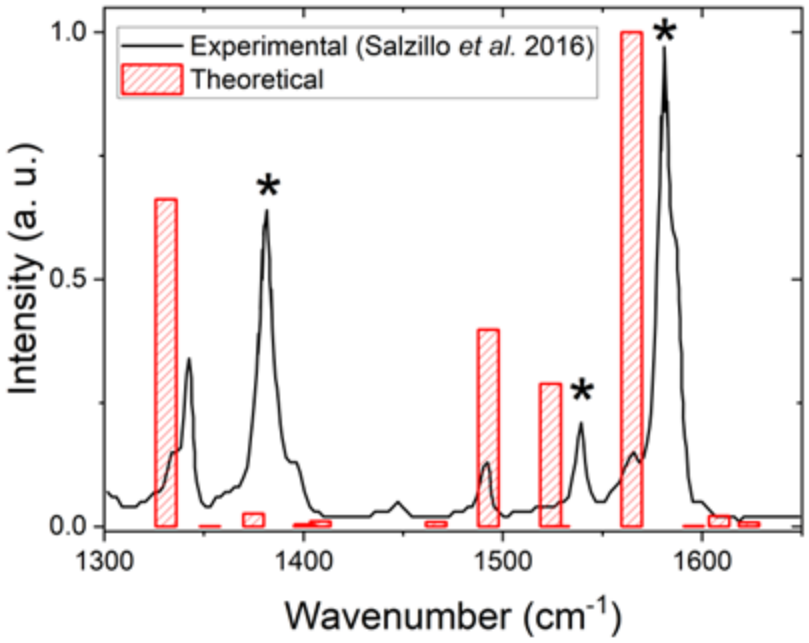

Figure 2. IR spectra of Pery:F4TCNQ CT complex, 1:1 stoichiometry. Black line is the experimental spectrum[20]. Red bar is the theoretical spectrum, calculated at the PBE(D3BJ)/PAW (plane wave) level of the theory. Asterisks labels, "*", underline bands which are considered for evaluating the experimental CT (see the text for details).

Figure 3 shows charge transfer values for the Pery:F4 complex as a function of both the level of the theory, and as a function of different approaches used in this work (Mulliken, Bader, DDEC6) to calculate localized atomic net charge values.

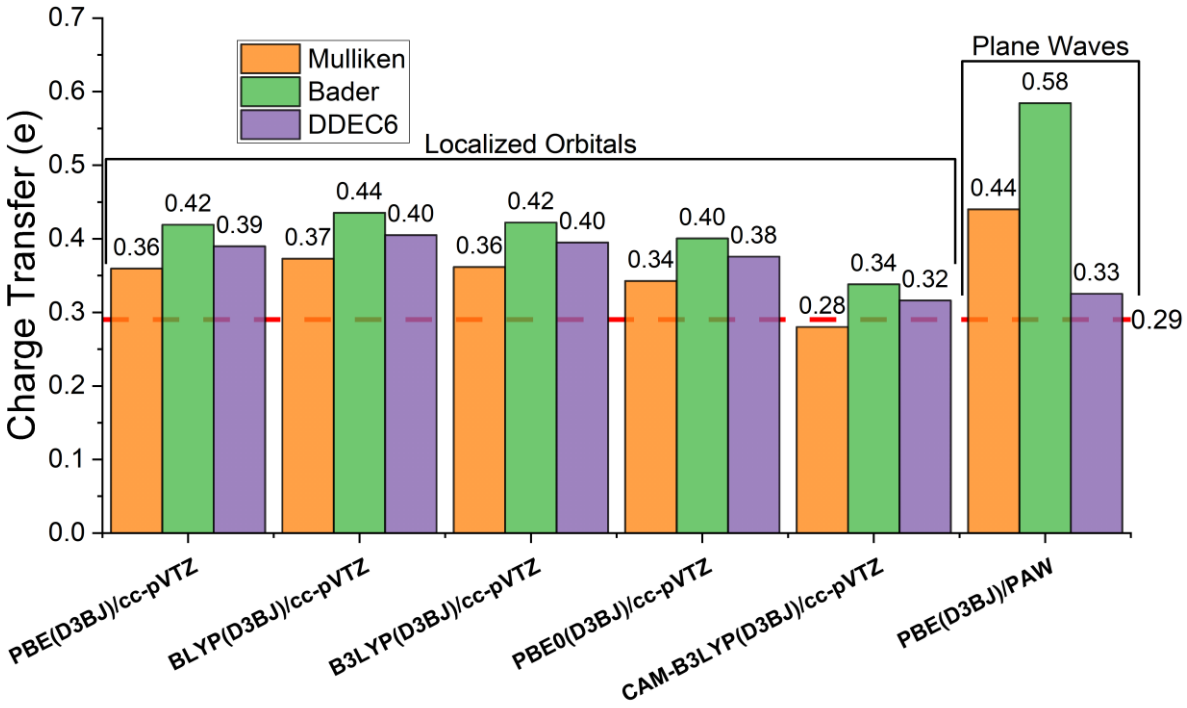

Figure 3. Calculated CT of Pery-F4_1:1 at various levels of theory employing Mulliken, Bader or DDEC6 population analysis.

It must be noted that i) there is a strong influence of the calculated CT value as a function of the quantum mechanical based paradigm. i.e. "localized orbitals", LO, vs. "plane wave", PW, Hamiltonians ii) also the strategy/scheme for electron density partition has a rather strong influence, the latter is an already well-known point in LO calculations where Löwdin and Mulliken "net charges" are recognized to yield substantially different results by varying the basis set, as they depend explicitly on the coefficients of the LCAO expansion. Indeed, this result seems especially evident for the Bader scheme population analysis, which seems to overestimate the ionicity of the system, as also reported in literature[65,66]. For instance, Bader values obtained within the LO paradigm appear rather in line with the experimental 0.29 electrons value (red dotted line in Fig 3), whilst PW values appear as rather unreliable, with about 50% error compared with the experimental value. Hence, on the basis of the results reported in Figure 3 the value of 0.29 electrons, obtained from the elaboration of experimental IR results, is in general agreement with theoretical results, especially with the one obtained at the higher level of theory (CAM-B3LYP(D3BJ)/cc-pVTZ). This saves for the Bader charges which yield values substantially different from the experimental estimation, and thus appear not suitable for evaluating CT values in molecular crystals, as the overestimated ionicity bias proper of the population analysis is compensated only by the long-range corrected functional. Despite that, Bader analysis is widely used in the field of PW calculations, and was already exploited to define the theoretical CT of similar system, leading to comparable results[27]; therefore, considering the results obtained from this

benchmark, the use of the Bader electron density decomposition for evaluate CT of molecular crystals from calculated electronic densities with PW is deplorable. Comparing the LO and the PW results shows that the main problem is the use of pseudopotentials that localize the core electrons on the centre of mass of atoms, introducing a non-ignorable error. The Mulliken net-charge scheme seems to work more efficiently when compared to Bader charges for PW for the same reason, as the LOBSTER protocol involves treating the core part with an auxiliary basis set, thus limiting the error introduced by pseudopotentials; in the same fashion, the DDEC6 method aims to correct the error due to the use of pseudopotential by exploiting a test electron density fitted to reproduce LO calculations. Moreover, the best performing exchange and correlation functional is the CAM-B3LYP, accounting for the minor ionicity and giving CTs of 0.28, 0.34, 0.32 electrons for Mulliken, Bader and DDEC6 respectively (experimental value 0.29 e). This performance is due to a more reliable reproduction of π-polarizability, the latter is a fundamental aspect in modelling CT π-complexes such the system under examination[67]. The influence of the basis set to the CT value was also investigated by benchmarking the impact of diffuse and polarization functions, all the results are reported in Table 1. As expected, the Mulliken population analysis does not converge approaching the complete basis set, with a non-physical value of 0.02 electrons for the most extended basis set tested (aug-cc-pVTZ) and an RMSD of 0.44 electrons. Both Bader and DDEC6 schemes performed well with an RMSD of, respectively, 0.17 and 0.12 electrons and maintaining the trend observed in Figure 3 with the Bader charges overestimating the ionicity in comparison to DDEC6. Another important observation is a major increasing in ionicity given by the addition of diffuse functions for Pople's basis sets. The same effect was observed for double-ζ Dunning's basis set, but not for its triple-ζ counterpart, with a change of only 0.01 electrons passing from cc-pVTZ to aug-cc-pVTZ. On the other hand, the effect of polarization functions seems to be minor with negligible difference passing from 6-31G, 6-31+G and 6-311++G(2d,2p) to 6-31G(d), 6-31+G(d), and 6-311++G(3df,3pd).

Table 1. Charge transfer (CT) of Pery-F4_1:1 evaluated varying the basis set and population analysis; the RMSD related to the experimental value is also reported.

Level of theory (CAM-B3LYP(D3BJ)/x)	Mulliken CT (e)	Bader CT (e)	DDEC6 CT (e)
6-31G	0.30	0.33	0.31
6-31+G	0.12	0.36	0.35
6-31G(d)	0.29	0.32	0.30
6-31+G(d)	0.51	0.36	0.34
6-311G(2d,2p)	0.27	0.33	0.31
6-311++G(2d,2p)	0.14	0.35	0.33
6-311++G(3df,3pd)	0.17	0.34	0.33
cc-pVDZ	0.26	0.31	0.29
aug-cc-pVDZ	0.46	0.35	0.33
cc-pVTZ	0.28	0.34	0.32

aug-cc-pVTZ	0.02	0.34	0.33
RMSD	0.47	0.17	0.12

Furthermore, to define the CT of Pery:F0 the DDEC6 population analysis was selected for both LO and PWs as it was the only reliable charge transfer value for PW Hamiltonian, and it has a lower basis set dependence for LO. In addition, as already observed in Figure 3, DDEC6 CTs were noticeably better than the ones evaluated with the Bader population analysis for all the functionals tested and the good agreement with the experimental value of Mulliken CTs is only ascribable to the choice of basis set.

Figure 4 sets out the IR and Raman spectra for the Pery:F0 CT complex (1:1 Stoichiometry). Figure 4A allows for a tight comparison between IR experimental and theoretical (calculated at the PBE(D3BJ)/PAW level of the theory) outcome, concerning in particular with the typical crystal fingerprint wavelength region, a reasonable agreement is found between experimental and theoretical results. On the contrary, the comparison between ref[26] experimental (estimated CT 0.0 electrons) and theoretical Raman spectra, reported in Figure S1, show a rather substantial difference. Indeed, due to the symmetry of the crystal, which is characterized by the presence of an inversion centre, the correct frequency match of IR active modes should bring to a correct match for the Raman spectrum too. This is probably related to the polarization of Raman spectra reported in ref[26], which brings a dependency between laser polarization and crystal orientation (that is not taken into account in the simulation, as the frequencies and intensities were evaluated at Γ). This could foreshadow that the reported CT of 0 electrons, i.e. no charge transfer, could not be correct. Thus, to verify this hypothesis, in this work three different Raman spectra obtained at different crystal orientations (Figure S2) were summed and compared to the theoretical (Figure 4B). Despite still not perfect, we achieved a better agreement between theoretical and experimental data (a comparison between ref[26] and polarization averaged spectra is reported in Figure S1 too). Frequencies of the theoretical Raman spectrum reported in Figure 4B, were scaled by 0.98. Which is a typical scaling factor recommended in the case of PBE calculations[68] (please note that unscaled frequencies are reported in Table S4). All experimental Raman intensities were converted in Raman activities thanks to Equation (1)[69–71];

$$A_i = I_i \frac{\nu_i(1 - \exp(-\frac{hc\nu_i}{kT})}{(\nu_0 - \nu_i)^4} \quad (1)$$

k, c, h are fundamental constants, ν_o is the laser frequency (cm^{-1}); ν_i is the vibrational frequency (cm^{-1}) of the ith normal mode, T is the temperature (K) and f is a suitably chosen common normalization factor for all peak intensities.

A)	B)

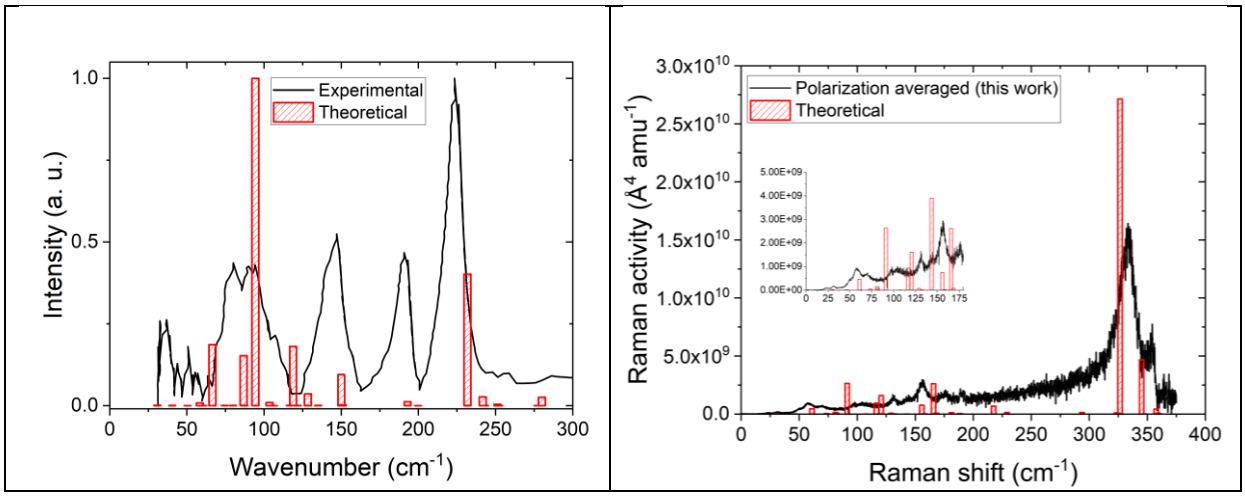

Figure 4. Pery:F0 CT crystal: A) IR spectra B) Raman spectra. Theoretical spectra are calculated at the PBE(D3BJ)/PAW level of the theory.

Concerning the calculated CT value for the Pery:F0 complex, Table 2 shows DDEC6 CT values calculated at the PBE(D3BJ)/PAW and CAM-B3LYP(D3BJ)/cc-pVTZ level of the theory. Which indeed are in close agreement with the experimental CT reported by Henderson[14] of 0.15 ± 0.05 electrons obtained both from IR spectroscopy and HOSE analysis[72].

Table 2. Calculated CT values, DDEC6 for Pery-F0_1:1. PBE(D3BJ)/PAW and CAM-B3LYP(D3BJ)/cc-pVTZ .

Level of theory	DDEC6 CT (e)	Experimental value by Henderson et al.[14] (e)	Experimental value by Vermeulen et al.[26] (e)
CAM-B3LYP(D3BJ)/cc-pVTZ†	0.16	0.15	0
PBE(D3BJ)/PAW‡	0.23		
† localized orbital basis set			
‡ plane wave basis set			

Thus, confirming a CT value equal to 0.15 ± 0.05 electrons, it is important to notice how the result of the PW basis set is slightly upper the experimental error. This hints how better results for low CT systems are given by extracting the D-A dimer and processing it with an LO basis set.

Figure 5 shows a comparison between the calculated spectrum and already published in the literature[14,20], the band marked ("*") was exploited to determine the experimental CT. The calculated frequencies are scaled by 1.02, as in Figure 2 (unscaled frequencies are reported in Table S4).

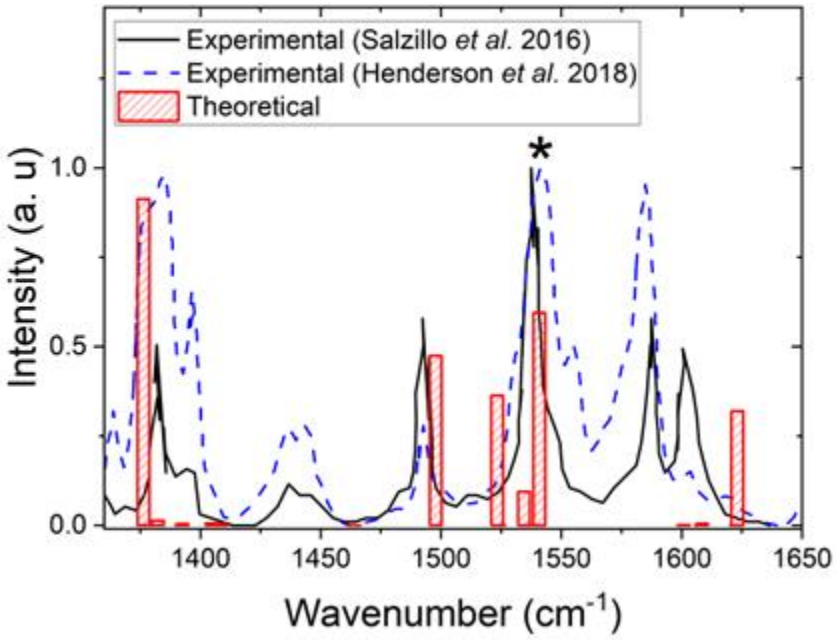

Figure 5. Pery:F0 CT crystal (1:1 stoichiometry), experimental IR spectra from refs[14,20]. Red bar is the theoretical spectrum calculated at the PBE(D3BJ)/PAW level of the theory. The band indicated by the asterisk, "*", is considered for the experimental estimation of the CT value.

Again, the charge transfer value determined by using a pseudopotential basis set yields a higher result than the experimental one, likely due to the overestimation on the ionicity of the system as a result of the use of pseudopotentials for core electrons. Charge sensitive intramolecular modes of F0 and F4 redshifted in comparison to experimental values. Hence, comparing the reference frequencies for the experimental determination of CT (Table S2), is clear how the amount of CT is related to the redshift of CT sensitive bands in the near-IR region. Thus, the overestimation of CT and the need of implementing a noncanonical scaling factor (1.02 was the scaling factor used in this work to correctly reproduce the charge sensitive frequencies) in order to obtain an acceptable match between spectra in the near-IR region at PBE(D3BJ)/PAW level of the theory and the experimental results are deeply linked and intrinsic on the usage of PAWs. The electronic properties of the two molecular crystals were also investigated in Figure 6**Figure** for both the Pery:F0 and Pery:F4 CT crystals the band plot along high symmetry points and density of states (DOS) are reported. For both species the DOS is dominated by the contribution of p orbitals, underlining once more the contribution of π-stacking interactions in the CT properties of Pery:FnTCNQ molecular crystals, confirming the need for better accounting the π-polarizability to model these systems. From the band plot it can be seen how Pery:F0 is a direct semiconductor with a bandgap of 390 meV at Γ, while Pery:F4 has two significant bandgaps one direct (223 meV at R) and one indirect (209 meV along X-R).

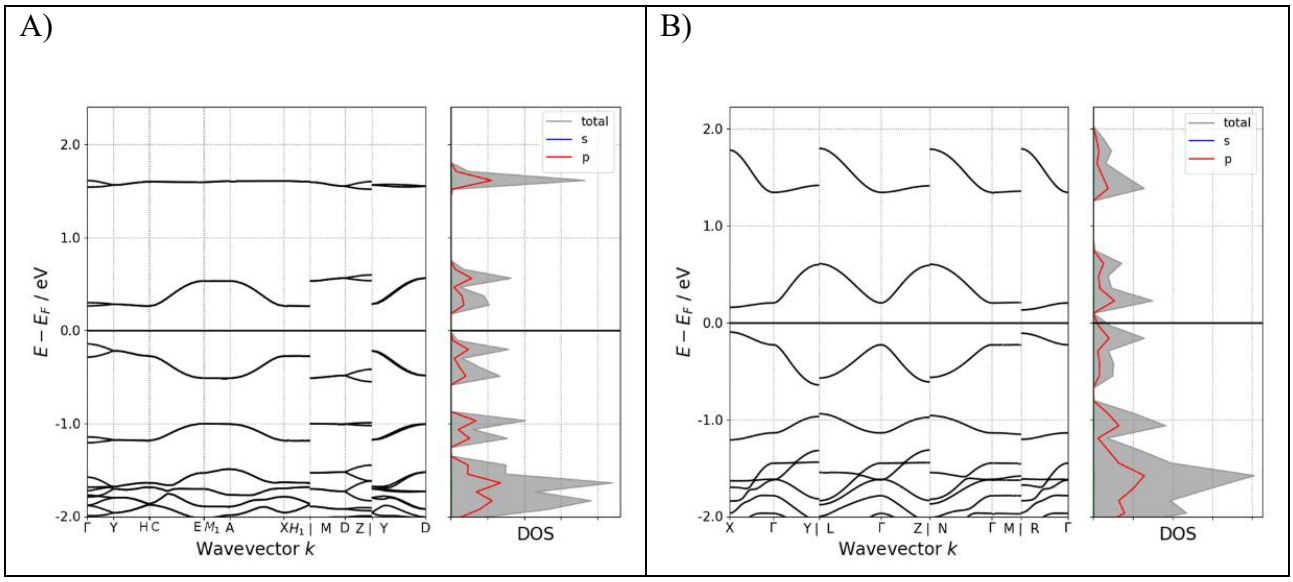

Figure 6. Band plot at high symmetry points and DOS, PBE(D3BJ)/PAW: A) Pery:F0 B) Pery:F4.

To characterize furthermore the conduction properties, the phonon localization was investigated by the participation ratio (PR)[73,74]; PR goes from 1 to 1/N (N=number of atoms), indicating with 1 modes where all the atoms of the unit cell are moving with the same amplitude (typically rigid translations) and with 1/N modes where only one atom is moving. The results for low frequency modes are displayed in Figure 7A for the Pery-F0 and in Figure 7B for the Pery-F4 (all PRs for each vibrational mode are reported in Table S3 and Table S4). This analysis led to the presence of more delocalized modes for Pery:F4 which, however, are shifted towards higher frequencies, leading to a minor occupation probability. This is important as highly delocalized vibrations are associated with killer phonon modes[74,75], that are responsible for decreasing charge mobility, increasing the thermal molecular disorder; those vibrational modes are indicated in Figure 7. In addition, the presence of highly delocalized phonons for Pery:F4 could promote the indirect semiconductor properties making the transition along X-R permitted.

A)	B)

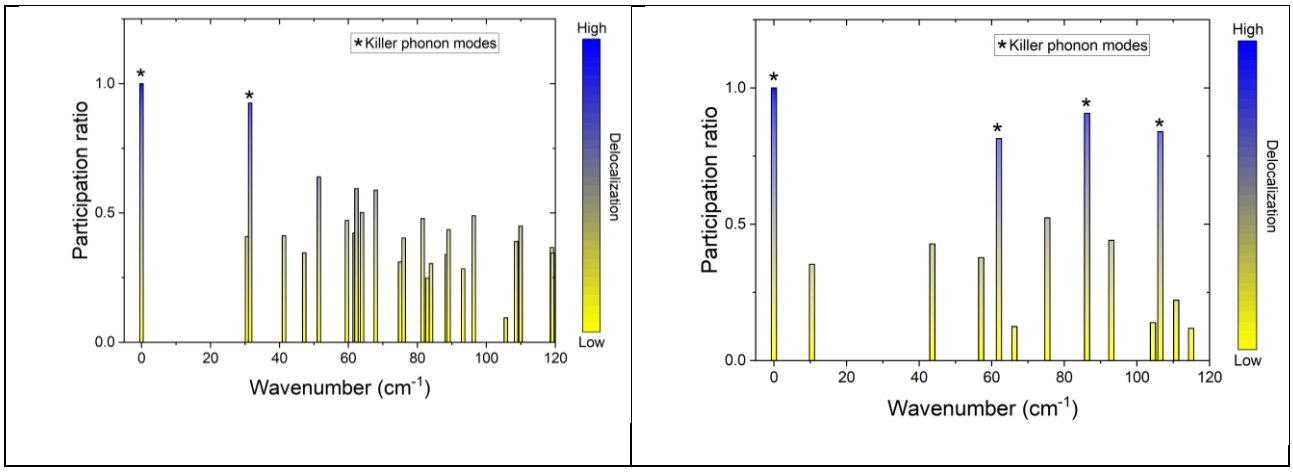

Figure 7. Participation ratio of low frequency vibrational modes: A) Pery:F0 B) Pery:F4; highly delocalized phonons (i.e. killer phonon) are marked with an asterisk ("*").

Conclusion

Different theoretical strategies devoted to the quantitative estimation of the degree of charge-transfer in donor-acceptor organic complexes have been systematically considered in this paper, with a focus on the Pery:FnTCNQ (n = 0, 4) charge transfer co-crystals. The CT values calculated with different strategies revealed marked differences. It must be noted that the widespread use PAW basis-set in conjunction with the Bader population analysis led to unreliable values, when dealing with CT π-complexes, even after the introduction of empirical dispersion corrections. Whilst the rather straightforward approach of extracting a D-A dimer from the periodic CT crystal structure, and the subsequent evaluation of the CT degree within localized orbital calculation framework, proved to be a legit methodology if it is coupled by a careful choice of population analysis and level of theory. Specifically, the CAM-B3LYP was the better performing functional tested in this work. Local hybrid and pure GGA functionals performed similarly to each other, overestimating the degree of CT, claiming the need of a long-range corrected hybrid functional to correctly describe the system. Furthermore, the influence of the basis set choice was investigated, finding an overestimation on the ionicity by adding diffuse functions (especially for Pople's split valence basis sets) and a negligible influence on the addition of polarization function. For PAW based calculations the problem lies in the overestimation of the ionicity of the system provided, which is caused by the exploitation of pseudopotentials (this is also reflected in the simulated Raman and IR spectra, where to compensate the ionicity overestimation an empirical scaling factor is needed). In addition, the representation of π-polarizability (the importance of which has been highlighted by DOS plots) is a known problem for both GGA and hybrid-GGA functionals, confirmed by the evidence that the best results in close agreement with the experimental results were obtained with a long-range corrected hybrid-GGA functional (CAM-B3LYP). DDEC6 charge density decomposition scheme was the better performing population

359 analysis, proving robust as exploited in various levels of the theory and giving acceptable results even
360 with the use of plane-wave calculations. The application of this work has allowed to confirm the CT
361 of Pery:TCNQ to be 0.15 and not 0. Finally, from the band structure and phonon delocalization anal-
362 ysis, the semiconductor nature of each system was underlined, with a greater expected charge mobil-
363 ity for Pery:F4TCNQ due the presence of killer phonon modes at higher energy compared to
364 Pery:TCNQ.

365

Acknowledgements

Financial support is gratefully acknowledged from Ministry of University and Research (MUR), PRIN 2022 cod. 2022NW4P2T "From metal nanoparticles to molecular complexes in electrocatalysis for green hydrogen evolution and simultaneous fine chemicals production (FUTURO)", PI Dr. Fracesco Vizza. Then, from Fondazione di Modena, Fondo di Ateneo per la Ricerca Anno 2023, linea FOMO, Progetto AMNESIA, PI Prof. Claudio Fontanesi. Financial support is also gratefully acknowledged from Consorzio Interuniversitario Nazionale per la Scienza e Tecnologia dei Materiali (INSTM), fondi triennali: "INSTM21MOFONTANESI". Authors acknowledge also financial support by Fondazione CR Firenze: Fondazione per la Ricerca e l'Innovazione dell'Università degli Studi di Firenze and Confindustria Firenze, FABER4 project framework.

T.S. thanks the Programma per Giovani Ricercatori "Rita Levi Montalcini" year 2020 (grant PGR20QN52R) of the Italian Ministry of University and Research (MUR) for the financial support. Project funded under the National Recovery and Resilience Plan (NRRP), Mission 04 Component 2 Investment 1.5─NextGenerationEU, call for tender no. 3277 dated 30/12/2021 (award number: 0001052 dated 23/06/2022).

References

(1) *Organic Electronics: Emerging Concepts and Technologies, Fabio Cicoira and Clara Santato Editors*; Wiley-VCH Verlag GmbH & Co. KGaA: Boschstr. 12, 69469 Weinheim, Germany, 2013.

(2) Vilan, A.; Yaffe, O.; Biller, A.; Salomon, A.; Kahn, A.; Cahen, D. Molecules on Si: Electronics with Chemistry. *Advanced Materials* **2010**, *22* (2), 140–159. https://doi.org/10.1002/adma.200901834.

(3) Hermerschmidt, F.; Choulis, S. A.; List-Kratochvil, E. J. W. Implementing Inkjet-Printed Transparent Conductive Electrodes in Solution-Processed Organic Electronics. *Advanced Materials Technologies* **2019**, *4* (5), 1800474. https://doi.org/10.1002/admt.201800474.

(4) Biscarini, F.; Coronado, E.; Painelli, A.; Yamashita, M. Materials for Molecular Electronics and Magnetism. *J. Mater. Chem. C* **2021**, *9* (33), 10521–10523. https://doi.org/10.1039/D1TC90161C.

(5) Bonechi, M.; Giurlani, W.; Stefani, A.; Marchetti, A.; Innocenti, M.; Fontanesi, C. Resorcinol Electropolymerization Process Obtained via Electrochemical Oxidation. *Electrochimica Acta* **2022**, *428*, 140928. https://doi.org/10.1016/j.electacta.2022.140928.

(6) King, B.; Lessard, B. H. Review of Recent Advances and Sensing Mechanisms in Solid-State Organic Thin-Film Transistor (OTFT) Sensors. *J. Mater. Chem. C* **2024**, *12* (16), 5654–5683. https://doi.org/10.1039/D3TC03611A.

(7) Chatterjee, O.; Roy, R.; Pramanik, A.; Dutta, T.; Sharma, V.; Sarkar, P.; Koner, A. L. Dynamic Self-Assembly of Photo-Reduced Perylene Diimide: Single-Component White Light Emission from Organic Radicals. *Advanced Optical Materials* **2022**, *10* (23), 2201187. https://doi.org/10.1002/adom.202201187.

(8) Morvillo, P.; Diana, R.; Fontanesi, C.; Ricciardi, R.; Lanzi, M.; Mucci, A.; Tassinari, F.; Schenetti, L.; Minarini, C.; Parenti, F. Low Band Gap Polymers for Application in Solar Cells: Synthesis and Characterization of Thienothiophene-Thiophene Copolymers. *Polym. Chem.* **2013**. https://doi.org/10.1039/C3PY01618H.

(9) Holliday, S.; Donaghey, J. E.; McCulloch, I. Advances in Charge Carrier Mobilities of Semiconducting Polymers Used in Organic Transistors. *Chem. Mater.* **2014**, *26* (1), 647–663. https://doi.org/10.1021/cm402421p.

(10) Chatterjee, O.; Biswas, S.; Pramanik, A.; Silswal, A.; Paliwal, B.; Koner, A. L. Position and Number Do Matter: Tuning Room Temperature Phosphorescence in Bromo-1,8-Naphthalimides through H-Aggregation and Halogen Bonding. *Advanced Optical Materials* **2024**, *12* (15), 2303069. https://doi.org/10.1002/adom.202303069.

(11) Goetz, K. P.; Vermeulen, D.; Payne, M. E.; Kloc, C.; McNeil, L. E.; Jurchescu, O. D. Charge-Transfer Complexes: New Perspectives on an Old Class of Compounds. *J. Mater. Chem. C* **2014**, *2* (17), 3065–3076. https://doi.org/10.1039/C3TC32062F.

(12) Shakya, S.; Khan, I. M. Charge Transfer Complexes: Emerging and Promising Colorimetric Real-Time Chemosensors for Hazardous Materials. *Journal of Hazardous Materials* **2021**, *403*, 123537. https://doi.org/10.1016/j.jhazmat.2020.123537.

(13) Pramanik, A.; Biswas, S.; Pal, S.; Sarkar, P. Charge Transport and Transfer Phenomena Involving Conjugated Acenes and Heteroacenes. *Bull Mater Sci* **2019**, *42* (3), 128. https://doi.org/10.1007/s12034-019-1781-9.

(14) Henderson, J.; Masino, M.; Hatcher, L. E.; Kociok-Köhn, G.; Salzillo, T.; Brillante, A.; Raithby, P. R.; Girlando, A.; Da Como, E. New Polymorphs of Perylene:Tetracyanoquinodimethane Charge Transfer Cocrystals. *Crystal Growth & Design* **2018**, *18* (4), 2003–2009. https://doi.org/10.1021/acs.cgd.7b01391.

(15) Zhang, C.; Wang, X.; Li, Y.; Sun, Y.; Zhang, Q. Spin in Organic Cocrystals. *Chemistry A European J* **2023**, *29* (32), e202300481. https://doi.org/10.1002/chem.202300481.

(16) Kaplan, I. G. *Theory of Molecular Interactions*; Studies in physical and theoretical chemistry; Elsevier: Amsterdam ; New York, 1986.

(17) Kitaigorodsky, A. *Molecular Crystals and Molecules*; Elsevier Science: Burlington, 2012.

(18) *Fundamentals of Crystallography*; Giacovazzo, C., Ed.; International Union of Crystallography texts on crystallography; Oxford University Press: Oxford ; New York, 2002.

(19) Huang, Y.; Ning, L.; Zhang, X.; Zhou, Q.; Gong, Q.; Zhang, Q. Stimuli-Fluorochromic Smart Organic Materials. *Chem. Soc. Rev.* **2024**, *53* (3), 1090–1166. https://doi.org/10.1039/D2CS00976E.

(20) Salzillo, T.; Masino, M.; Kociok-Köhn, G.; Di Nuzzo, D.; Venuti, E.; Della Valle, R. G.; Vanossi, D.; Fontanesi, C.; Girlando, A.; Brillante, A.; Da Como, E. Structure, Stoichiometry, and Charge Transfer in Cocrystals of Perylene with TCNQ-F $_x$. *Crystal Growth & Design* **2016**, *16* (5), 3028–3036. https://doi.org/10.1021/acs.cgd.5b01663.

(21) Biswas, S.; Pramanik, A.; Pal, S.; Sarkar, P. A Theoretical Perspective on the Photovoltaic Performance of S,N-Heteroacenes: An Even–Odd Effect on the Charge Separation Dynamics. *J. Phys. Chem. C* **2017**, *121* (5), 2574–2587. https://doi.org/10.1021/acs.jpcc.6b11471.

(22) Voityuk, A. A. Electronic Coupling for Charge Transfer in Donor–Bridge–Acceptor Systems. Performance of the Two-State FCD Model. *Phys. Chem. Chem. Phys.* **2012**, *14* (40), 13789. https://doi.org/10.1039/c2cp40579b.

(23) Gao, J.; Zhai, H.; Hu, P.; Jiang, H. The Stoichiometry of TCNQ-Based Organic Charge-Transfer Cocrystals. *Crystals* **2020**, *10* (11), 993. https://doi.org/10.3390/cryst10110993.

(24) Anderson, M.; Ramanan, C.; Fontanesi, C.; Frick, A.; Surana, S.; Cheyns, D.; Furno, M.; Keller, T.; Allard, S.; Scherf, U.; Beljonne, D.; D'Avino, G.; Von Hauff, E.; Da Como, E. Displacement of Polarons by Vibrational Modes in Doped Conjugated Polymers. *Phys. Rev. Materials* **2017**, *1* (5), 055604. https://doi.org/10.1103/PhysRevMaterials.1.055604.

(25) Vanossi, D.; Cigarini, L.; Giaccherini, A.; Da Como, E.; Fontanesi, C. An Integrated Experimental/Theoretical Study of Structurally Related Poly-Thiophenes Used in Photovoltaic Systems. *Molecules* **2016**, *21* (1), 110. https://doi.org/10.3390/molecules21010110.

(26) Vermeulen, D.; Zhu, L. Y.; Goetz, K. P.; Hu, P.; Jiang, H.; Day, C. S.; Jurchescu, O. D.; Coropceanu, V.; Kloc, C.; McNeil, L. E. Charge Transport Properties of Perylene–TCNQ Crystals: The Effect of Stoichiometry. *J. Phys. Chem. C* **2014**, *118* (42), 24688–24696. https://doi.org/10.1021/jp508520x.

(27) Solano, F.; Inaudi, P.; Abollino, O.; Giacomino, A.; Chiesa, M.; Salvadori, E.; Kociok-Kohn, G.; da Como, E.; Salzillo, T.; Fontanesi, C. Charge Transfer Modulation in Charge Transfer Co-Crystals Driven by Crystal Structure Morphology. *Physical Chemistry Chemical Physics* **2022**, *24* (31), 18816–18823. https://doi.org/10.1039/d2cp01408d.

(28) Zhu, W.; Yi, Y.; Zhen, Y.; Hu, W. Precisely Tailoring the Stoichiometric Stacking of Perylene-TCNQ Co-Crystals towards Different Nano and Microstructures with Varied Optoelectronic Performances. *Small* **2015**, *11* (18), 2150–2156. https://doi.org/10.1002/smll.201402330.

(29) Wu, H.-D.; Peng, H.-D.; Pan, G.-B. Precise Growth of Low-Dimensional pyrene·perylene·TCNQ Co-Crystals and Structure–Property Related Optoelectronic Properties. *RSC Adv.* **2016**, *6* (82), 78979–78983. https://doi.org/10.1039/C6RA17200H.

(30) Shokaryev, I.; Buurma, A. J. C.; Jurchescu, O. D.; Uijttewaal, M. A.; De Wijs, G. A.; Palstra, T. T. M.; De Groot, R. A. Electronic Band Structure of Tetracene−TCNQ and Perylene−TCNQ Compounds. *J. Phys. Chem. A* **2008**, *112* (11), 2497–2502. https://doi.org/10.1021/jp0753777.

(31) Salzillo, T.; Della Valle, R. G.; Venuti, E.; Kociok-Köhn, G.; Masino, M.; Girlando, A.; Brillante, A. Solution Equilibrium between Two Structures of Perylene-F2TCNQ Charge Transfer Co-Crystals. *Journal of Crystal Growth* **2019**, *516*, 45–50. https://doi.org/10.1016/j.jcrysgro.2019.03.026.

(32) Kumar, A.; Banerjee, K.; Ervasti, M. M.; Kezilebieke, S.; Dvorak, M.; Rinke, P.; Harju, A.; Liljeroth, P. Electronic Characterization of a Charge-Transfer Complex Monolayer on Graphene. *ACS Nano* **2021**, *15* (6), 9945–9954. https://doi.org/10.1021/acsnano.1c01430.

(33) Doan Truong, K.; Bandrauk, A. D. A New TCNQ Complex: (Perylene)3 TCNQ. *Chemical Physics Letters* **1976**, *44* (2), 232–235. https://doi.org/10.1016/0009-2614(76)80497-6.

(34) Bandrauk, A. D.; Truong, K. D.; Carlone, C. Optical and Raman spectra of single crystals of perylene-TCNQ charge transfer complexes. *Can. J. Chem.* **1982**, *60* (5), 588–595. https://doi.org/10.1139/v82-087.

(35) Solano, F.; Inaudi, P.; Chiesa, M.; Kociok-Köhn, G.; Salvadori, E.; Da Como, E.; Vanossi, D.; Malandrino, M.; Carmieli, R.; Giacomino, A.; Fontanesi, C. Spin Multiplicity and Solid-State Electrochemical Behavior in Charge-Transfer Co-Crystals of DBTTF/F4TCNQ. *J. Phys. Chem. C* **2021**, *125* (16), 8677–8683. https://doi.org/10.1021/acs.jpcc.1c00020.

(36) Salzillo, T.; Marchetti, A.; Vejpravova, J.; Fanjul Bolado, P.; Fontanesi, C. Molecular Electrochemistry. An Overview of a Cross-Field: Electrochemistry/Spectroscopic/Theoretical Integrated Approach. *Current Opinion in Electrochemistry* **2022**, *35*, 101072. https://doi.org/10.1016/j.coelec.2022.101072.

(37) Kresse, G.; Furthmüller, J. Efficiency of Ab-Initio Total Energy Calculations for Metals and Semiconductors Using a Plane-Wave Basis Set. *Computational Materials Science* **1996**, *6* (1), 15–50. https://doi.org/10.1016/0927-0256(96)00008-0.

(38) Kresse, G.; Furthmüller, J. Efficient Iterative Schemes for *Ab Initio* Total-Energy Calculations Using a Plane-Wave Basis Set. *Phys. Rev. B* **1996**, *54* (16), 11169–11186. https://doi.org/10.1103/PhysRevB.54.11169.

(39) Kresse, G.; Hafner, J. Norm-Conserving and Ultrasoft Pseudopotentials for First-Row and Transition Elements. *J. Phys.: Condens. Matter* **1994**, *6* (40), 8245–8257. https://doi.org/10.1088/0953-8984/6/40/015.

(40) Kresse, G.; Joubert, D. From Ultrasoft Pseudopotentials to the Projector Augmented-Wave Method. *Phys. Rev. B* **1999**, *59* (3), 1758–1775. https://doi.org/10.1103/PhysRevB.59.1758.

(41) Perdew, J. P.; Burke, K.; Ernzerhof, M. Generalized Gradient Approximation Made Simple [Phys. Rev. Lett. 77, 3865 (1996)]. *Phys. Rev. Lett.* **1997**, *78* (7), 1396–1396. https://doi.org/10.1103/PhysRevLett.78.1396.

(42) Grimme, S.; Ehrlich, S.; Goerigk, L. Effect of the Damping Function in Dispersion Corrected Density Functional Theory. *J Comput Chem* **2011**, *32* (7), 1456–1465. https://doi.org/10.1002/jcc.21759.

(43) Togo, A.; Tanaka, I. First Principles Phonon Calculations in Materials Science. *Scripta Materialia* **2015**, *108*, 1–5. https://doi.org/10.1016/j.scriptamat.2015.07.021.

(44) Skelton, J. M.; Burton, L. A.; Jackson, A. J.; Oba, F.; Parker, S. C.; Walsh, A. Lattice Dynamics of the Tin Sulphides SnS_2, SnS and Sn_2S_3: Vibrational Spectra and Thermal Transport. *Phys. Chem. Chem. Phys.* **2017**, *19* (19), 12452–12465. https://doi.org/10.1039/C7CP01680H.

(45) M. J. Frisch, G. W. Trucks, H. B. Schlegel, G. E. Scuseria, M. A. Robb, J. R. Cheeseman, G. Scalmani, V. Barone, G. A. Petersson, H. Nakatsuji, X. Li, M. Caricato, A. V. Marenich, J. Bloino, B. G. Janesko, R. Gomperts, B. Mennucci, H. P. Hratchian, J. V. Ortiz, A. F. Izmaylov, J. L. Sonnenberg, D. Williams-Young, F. Ding, F. Lipparini, F. Egidi, J. Goings, B. Peng, A. Petrone, T. Henderson, D. Ranasinghe, V. G. Zakrzewski, J. Gao, N. Rega, G. Zheng, W. Liang, M. Hada, M. Ehara, K. Toyota, R. Fukuda, J. Hasegawa, M. Ishida, T. Nakajima, Y. Honda, O. Kitao, H. Nakai, T. Vreven, K. Throssell, J. A. Montgomery, Jr., J. E. Peralta, F. Ogliaro, M. J. Bearpark, J. J. Heyd, E. N. Brothers, K. N. Kudin, V. N. Staroverov, T. A. Keith, R. Kobayashi, J. Normand, K. Raghavachari, A. P. Rendell, J. C. Burant, S. S. Iyengar, J. Tomasi, M. Cossi, J. M. Millam, M. Klene, C. Adamo, R. Cammi, J. W. Ochterski, R. L. Martin, K. Morokuma, O. Farkas, J. B. Foresman, and D. J. Gaussian 16, Revision B.01, 2016.

(46) Manz, T. A.; Limas, N. G. Introducing DDEC6 Atomic Population Analysis: Part 1. Charge Partitioning Theory and Methodology. *RSC Adv.* **2016**, *6* (53), 47771–47801. https://doi.org/10.1039/C6RA04656H.
(47) Maintz, S.; Deringer, V. L.; Tchougréeff, A. L.; Dronskowski, R. LOBSTER: A Tool to Extract Chemical Bonding from Plane-wave Based DFT. *J Comput Chem* **2016**, *37* (11), 1030–1035. https://doi.org/10.1002/jcc.24300.
(48) Tang, W.; Sanville, E.; Henkelman, G. A Grid-Based Bader Analysis Algorithm without Lattice Bias. *J. Phys.: Condens. Matter* **2009**, *21* (8), 084204. https://doi.org/10.1088/0953-8984/21/8/084204.
(49) Yu, M.; Trinkle, D. R. Accurate and Efficient Algorithm for Bader Charge Integration. *The Journal of Chemical Physics* **2011**, *134* (6), 064111. https://doi.org/10.1063/1.3553716.
(50) Lu, T.; Chen, F. Multiwfn: A Multifunctional Wavefunction Analyzer. *J Comput Chem* **2012**, *33* (5), 580–592. https://doi.org/10.1002/jcc.22885.
(51) Yanai, T.; Tew, D. P.; Handy, N. C. A New Hybrid Exchange–Correlation Functional Using the Coulomb-Attenuating Method (CAM-B3LYP). *Chemical Physics Letters* **2004**, *393* (1–3), 51–57. https://doi.org/10.1016/j.cplett.2004.06.011.
(52) Kendall, R. A.; Dunning, T. H.; Harrison, R. J. Electron Affinities of the First-Row Atoms Revisited. Systematic Basis Sets and Wave Functions. *The Journal of Chemical Physics* **1992**, *96* (9), 6796–6806. https://doi.org/10.1063/1.462569.
(53) Miehlich, B.; Savin, A.; Stoll, H.; Preuss, H. Results Obtained with the Correlation Energy Density Functionals of Becke and Lee, Yang and Parr. *Chemical Physics Letters* **1989**, *157* (3), 200–206. https://doi.org/10.1016/0009-2614(89)87234-3.
(54) Becke, A. D. Density-Functional Thermochemistry. III. The Role of Exact Exchange. *The Journal of Chemical Physics* **1993**, *98* (7), 5648–5652. https://doi.org/10.1063/1.464913.
(55) Adamo, C.; Barone, V. Toward Reliable Density Functional Methods without Adjustable Parameters: The PBE0 Model. *The Journal of Chemical Physics* **1999**, *110* (13), 6158–6170. https://doi.org/10.1063/1.478522.
(56) Ditchfield, R.; Hehre, W. J.; Pople, J. A. Self-Consistent Molecular-Orbital Methods. IX. An Extended Gaussian-Type Basis for Molecular-Orbital Studies of Organic Molecules. *The Journal of Chemical Physics* **1971**, *54* (2), 724–728. https://doi.org/10.1063/1.1674902.
(57) Frisch, M. J.; Pople, J. A.; Binkley, J. S. Self-Consistent Molecular Orbital Methods 25. Supplementary Functions for Gaussian Basis Sets. *The Journal of Chemical Physics* **1984**, *80* (7), 3265–3269. https://doi.org/10.1063/1.447079.
(58) Clark, T.; Chandrasekhar, J.; Spitznagel, G. W.; Schleyer, P. V. R. Efficient Diffuse Function-augmented Basis Sets for Anion Calculations. III. The 3-21+G Basis Set for First-row Elements, Li–F. *J Comput Chem* **1983**, *4* (3), 294–301. https://doi.org/10.1002/jcc.540040303.
(59) Krishnan, R.; Binkley, J. S.; Seeger, R.; Pople, J. A. Self-Consistent Molecular Orbital Methods. XX. A Basis Set for Correlated Wave Functions. *The Journal of Chemical Physics* **1980**, *72* (1), 650–654. https://doi.org/10.1063/1.438955.
(60) Dunning, T. H. Gaussian Basis Sets for Use in Correlated Molecular Calculations. I. The Atoms Boron through Neon and Hydrogen. *The Journal of Chemical Physics* **1989**, *90* (2), 1007–1023. https://doi.org/10.1063/1.456153.
(61) Nanova, D.; Beck, S.; Fuchs, A.; Glaser, T.; Lennartz, C.; Kowalsky, W.; Pucci, A.; Kroeger, M. Charge Transfer in Thin Films of Donor–Acceptor Complexes Studied by Infrared Spectroscopy. *Organic Electronics* **2012**, *13* (7), 1237–1244. https://doi.org/10.1016/j.orgel.2012.02.021.
(62) Girlando, A.; Painelli, A.; Pecile, C. Electron-Intramolecular Phonon Coupling in Regular and Dimerized Mixed Stack Organic Semiconductors. *Molecular Crystals and Liquid Crystals* **1985**, *120* (1), 17–26. https://doi.org/10.1080/00268948508075754.
(63) Painelli, A.; Girlando, A. Electron–Molecular Vibration (e–Mv) Coupling in Charge-Transfer Compounds and Its Consequences on the Optical Spectra: A Theoretical Framework. *The Journal of Chemical Physics* **1986**, *84* (10), 5655–5671. https://doi.org/10.1063/1.449926.
(64) Kato, Y.; Matsumoto, H.; Mori, T. Absence of HOMO/LUMO Transition in Charge-Transfer Complexes of Thienoacenes. *J. Phys. Chem. A* **2021**, *125* (1), 146–153. https://doi.org/10.1021/acs.jpca.0c08925.

(65) Han, B.; Isborn, C. M.; Shi, L. Determining Partial Atomic Charges for Liquid Water: Assessing Electronic Structure and Charge Models. *J. Chem. Theory Comput.* **2021**, *17* (2), 889–901. https://doi.org/10.1021/acs.jctc.0c01102.
(66) Sotoudeh, M.; Baumgart, S.; Dillenz, M.; Döhn, J.; Forster-Tonigold, K.; Helmbrecht, K.; Stottmeister, D.; Groß, A. Ion Mobility in Crystalline Battery Materials. *Advanced Energy Materials* **2024**, *14* (4), 2302550. https://doi.org/10.1002/aenm.202302550.
(67) Kodikara, M. S.; Stranger, R.; Humphrey, M. G. Long-Range Corrected DFT Calculations of First Hyperpolarizabilities and Excitation Energies of Metal Alkynyl Complexes. *ChemPhysChem* **2018**, *19* (12), 1537–1546. https://doi.org/10.1002/cphc.201701052.
(68) Alecu, I. M.; Zheng, J.; Zhao, Y.; Truhlar, D. G. Computational Thermochemistry: Scale Factor Databases and Scale Factors for Vibrational Frequencies Obtained from Electronic Model Chemistries. *J. Chem. Theory Comput.* **2010**, *6* (9), 2872–2887. https://doi.org/10.1021/ct100326h.
(69) Muniz-Miranda, F.; Pedone, A.; Muniz-Miranda, M. Raman and Computational Study on the Adsorption of Xanthine on Silver Nanocolloids. *ACS Omega* **2018**, *3* (10), 13530–13537. https://doi.org/10.1021/acsomega.8b02174.
(70) Krishnakumar, V.; Keresztury, G.; Sundius, T.; Seshadri, S. Density Functional Theory Study of Vibrational Spectra and Assignment of Fundamental Vibrational Modes of 1-Methyl-4-Piperidone. *Spectrochimica Acta Part A: Molecular and Biomolecular Spectroscopy* **2007**, *68* (3), 845–850. https://doi.org/10.1016/j.saa.2006.12.069.
(71) Muniz-Miranda, M.; Gellini, C.; Pagliai, M.; Innocenti, M.; Salvi, P. R.; Schettino, V. SERS and Computational Studies on MicroRNA Chains Adsorbed on Silver Surfaces. *J. Phys. Chem. C* **2010**, *114* (32), 13730–13735. https://doi.org/10.1021/jp103304r.
(72) Dobrowolski, M. A.; Garbarino, G.; Mezouar, M.; Ciesielski, A.; Cyrański, M. K. Structural Diversities of Charge Transfer Organic Complexes. Focus on Benzenoid Hydrocarbons and 7,7,8,8-Tetracyanoquinodimethane. *CrystEngComm* **2014**, *16* (3), 415–429. https://doi.org/10.1039/C3CE41703D.
(73) Jiang, P.; Hu, S.; Ouyang, Y.; Ren, W.; Yu, C.; Zhang, Z.; Chen, J. Remarkable Thermal Rectification in Pristine and Symmetric Monolayer Graphene Enabled by Asymmetric Thermal Contact. *Applied Physics* **2020**.
(74) Kamencek, T.; Zojer, E. Discovering Structure–Property Relationships for the Phonon Band Structures of Hydrocarbon-Based Organic Semiconductor Crystals: The Instructive Case of Acenes. *J. Mater. Chem. C* **2022**, *10* (7), 2532–2543. https://doi.org/10.1039/D1TC04708F.
(75) Schweicher, G.; D'Avino, G.; Ruggiero, M. T.; Harkin, D. J.; Broch, K.; Venkateshvaran, D.; Liu, G.; Richard, A.; Ruzié, C.; Armstrong, J.; Kennedy, A. R.; Shankland, K.; Takimiya, K.; Geerts, Y. H.; Zeitler, J. A.; Fratini, S.; Sirringhaus, H. Chasing the "Killer" Phonon Mode for the Rational Design of Low-Disorder, High-Mobility Molecular Semiconductors. *Advanced Materials* **2019**, *31* (43), 1902407. https://doi.org/10.1002/adma.201902407.